Chemosphere 346 (2024) 140600

Contents lists available at ScienceDirect

Chemosphere

journal homepage: www.elsevier.com/locate/chemosphere

Adsorption of per- and polyfluoroalkyl substances (PFAS) from water with porous organic polymers

Yan Zhang [a], Bin Wang [b], Shengqian Ma [b], Qiong Zhang [a,*]

[a] Department of Civil and Environmental Engineering, University of South Florida, USA
[b] Department of Chemistry, University of North Texas, USA

HIGHLIGHTS

- Cationic POP shows a fast adsorption rate and a high capacity for PFAS removal.
- The designed POP maintained above 85% removal for PFBA at a pH range of 5–9.
- The effect of the co-contaminants on PFBA removal followed the order of HA > PFOS > Cl^-.
- PFAS removal maintained at 90% in five consecutive adsorption/regeneration cycles.

GRAPHICAL ABSTRACT

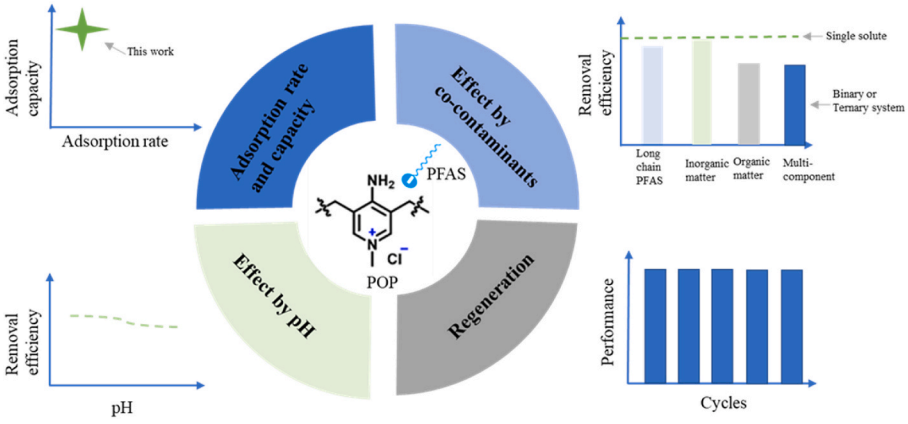

ARTICLE INFO

Handling editor: Y Yeomin Yoon

Keywords:
Short-chain PFAS
Porous organic polymer
Kinetics
Single and multicomponent isotherms
Regeneration

ABSTRACT

Per- and polyfluoroalkyl substances (PFAS) are man-made environmental contaminants causing increasing global concern due to their adverse effect on environmental and human health. Conventional treatment methods are ineffective in removing short-chain PFAS because they are persistent and recalcitrant to treatment. This study evaluated the performance of a structurally-tunable and chemically-stable porous organic polymer (POP) for PFAS removal under realistic environmental conditions. The POP demonstrated an exceptionally high removal efficiency (>95%) within 15 min when the initial PFAS concentration was approximately 400 ng/L. The adsorption of PFAS on the POP was not significantly affected by changes in solution pH within the range of 5–9. The common co-contaminants in water competed with short-chain PFAS for active sites during the adsorption process following the order of natural organic matter (NOM), long-chain PFAS, and Cl^-. The Freundlich-type model could predict the multicomponent interactions well with a R^2 value above 0.91. The spent POP was effectively regenerated using a mixture of the 10% NaCl and 30% methanol solution and the PFAS removal maintained at 90% through five adsorption and desorption cycles. The characteristics of the designed POP make it a highly promising and stable absorbent. It enables fast and effective removal of short-chain PFAS.

* Corresponding author. 4202 E. Fowler Avenue, ENG 030, University of South Florida, Tampa, FL, 33620-5350, USA.
E-mail address: qiongzhang@usf.edu (Q. Zhang).

https://doi.org/10.1016/j.chemosphere.2023.140600
Received 2 August 2023; Received in revised form 29 October 2023; Accepted 30 October 2023
Available online 31 October 2023

1. Introduction

Per- and polyfluoroalkyl substances (PFAS) are a broad category of man-made environmental contaminants causing increasing global concern due to their adverse effect on environmental and human health. These compounds belong to a broad category of synthetic chemicals. Their structure usually consists of 4–12 carbons atoms in length, and all hydrogen atoms have been replaced by fluorine (Lau et al., 2007). PFAS are divided into two categories based on the length of the carbon chain. Perfluorocarboxylic acids (PFCAs) with less than 8 carbon atoms and perfluoroalkane sulfonic acids (PFSAs) with less than 6 carbon atoms are short-chain PFAS (Brendel et al., 2018).

The carbon-fluorine (C–F) bonds are highly polar and strong, leading to PFAS thermal and chemical stability (Verma et al., 2022). PFAS display hydrophilic and hydrophobic properties due to the functional hydrophilic group head and the hydrophobic C–F tail (Meegoda et al., 2020). The unique features of PFAS make them suitable for many industrial applications, such as household products, industrial products, flame retardants, and waterproof clothing (Fujii et al., 2007; Houtz et al., 2013). Therefore, their presence in the environment is widespread. The U.S. Environmental Protection Agency (U.S. EPA) has proposed regulations that establish maximum contaminant levels (MCLs) for perfluorooctanesulfonic acid (PFOS) and perfluorooctanoic acid (PFOA) at a concentration of four ng/L (U.S. EPA, 2023).

Conventional coagulation, flocculation, and sedimentation processes are ineffective for PFAS removal due to their thermal and chemical stability (Ateia et al., 2019). Various treatment methods have been explored, such as advanced oxidation processes (AOPs) (Espana et al., 2015), sonolysis (Moldes et al., 2005), high-pressure membranes (Dickenson and Higgins, 2016), and adsorption (Zhang et al., 2019). However, many of these treatment techniques are expensive because of the high energy or capital cost requirements, as well as the potential for generating a large amount of waste (Kucharzyk et al., 2017). Among them, adsorption has been shown to be a highly promising method for removing PFAS from aquatic environment because of its simplicity, relatively low cost, and high removal efficiency (Gagliano et al., 2020; Crone et al., 2019). The PFAS concentrated on an adsorbent can be desorbed during regeneration that produces a waste stream at a relatively small volume. The PFAS present at high concentrations in the waste stream can be further destructed through some technologies including sonochemical, electrochemical oxidation, and thermal degradation/incineration (Meegoda et al., 2022). The predominant mechanisms for PFAS adsorption are hydrophobic and electrostatic interactions, while hydrogen bonding, covalent bonding, and van der Waals are less important (Wu et al., 2020). Effective removal of PFAS has been demonstrated using a range of adsorbents, including anion exchange resin (Zhang et al., 2019), biomaterials (Deng et al., 2013), polymers (Karoyo and Wilson, 2013), mineral materials (Punyapalakul et al., 2013), carbon nanotubes (CNTs) (Yang and Xing, 2010), and activated carbon (AC) (Rattanaoudom et al., 2012).

Previous studies demonstrated that granular activated carbon (GAC) and other conventional adsorbents are effective in removing long-chain PFAS (Chularueangaksorn et al., 2014; Senevirathna, 2010; Rattanaoudom et al., 2012); however, they are non-selective, and the removal efficiency for short-chain PFAS is low (Brendel et al., 2018). This is because short-chain PFAS have higher hydrophilicity compared with long-chain PFAS (Li et al., 2020). In addition, the majority of the published experimental studies were conducted under high concentrations of PFAS (high μg/L to high mg/L) spiked in water (Maimaiti et al., 2018; Wang et al., 2016) which are not common in typical aquatic environment. The concentrations of PFAS in surface water and groundwater are typically in the low ng/L to low μg/L range. Therefore, there is a need to develop more efficient adsorbents, including high capacities, fast uptake kinetics, and high selectivity for short-chain PFAS under realistic environmental conditions.

The structures of PFAS contain the hydrophilic head of carboxylic or sulfonic groups that become deprotonated in water, and the hydrophobic tail of $–CF_2$- chain. Therefore, an adsorbent with cationic nanotraps capable of selectively capturing the anionic carboxylic or sulfonic groups and functional groups capable of forming hydrogen bonding interactions with the $–CF_2$- groups is ideal for short-chain PFAS removal from water. Additionally, adsorbents with high surface area, large pore size, and flexible framework, which facilitate mass transfer, are also highly desirable. Porous organic polymers (POPs) are a type of material with a highly porous structure composed of organic building blocks (Zhang et al., 2020). The unique characteristics of POPs, such as high surface area, adjustable framework structure, and exceptional water/-chemical stabilities render them as promising candidate materials for PFAS removal (Li et al., 2014; Zhang et al., 2020). For example, POPs have achieved 99.99% removal efficiency for PFOA within 2 min at an initial concentration of 1 mg/L (Liu et al., 2022b). However, the application of POPs for short-chain PFAS removal is underexplored. Furthermore, many co-contaminants in the aquatic environment can affect adsorption performance. Most current research has been limited to a preliminary laboratory assessment of adsorption performance without considering the influence of co-contaminants on short-chain PFAS removal using the POPs. Finally, there is no study examining the proper regeneration condition for POPs to be reused in water treatment applications.

Therefore, the goal of this study is to evaluate the performance of a structurally-tunable and chemically-stable POP for PFAS removal at environmentally relevant concentrations and conditions. The POP was developed by simultaneously incorporating electrostatic and hydrogen-bonding sites into the pores of the POP. Such dual-functional POP can synergistically and efficiently bind short-chain PFAS molecules at the molecular level. This study was designed to investigate the adsorption capacity, adsorption rate, the effect of pH and co-contaminants, and recyclability of the developed POP. This multifaceted approach not only enhances the novelty of this research but also underscores its practical applications in addressing real-world environmental challenges. The results of this study provide insight into the applicability of emerging adsorbent as an efficient treatment method for PFAS removal at environmentally relevant concentrations and conditions.

2. Material and methods

2.1. PFAS stock solutions and reagents

This study selected a total of 5 PFAS as representatives for long-chain and short-chain in the common water sources. Specifically, PFOS was selected to represent the long-chain PFAS; PFBS, PFBA, PFHxA, and PFHpA were selected to represent short-chain PFAS. All PFAS and mass-labeled standards were ordered from Wellington Laboratories Inc., Ontario, Canada (Table S1). All other solvents and reagents were ordered from Sigma-Aldrich of suitable analytical grade and high purity.

2.2. Adsorbent materials

The short-chain PFAS adsorbent, PQA-pNH_2Py-Cl, was obtained by methylating the pyridine-based POP, POP-pNH_2Py, functionalized with amino groups on the para-position, using CH_3I as the reagent, followed by ion exchange with NaCl solution. The synthesis of PQA-*p*NH_2Py-Cl followed our previous work with some modifications (details are shown in the Supporting Information) (Sun et al., 2019). The organic building block, 3,5-divinylpyridin-4-amine, was synthesized based on the Suzuki coupling reaction between 3,5-dibromopyridin-4-amine and potassium vinyltrifluoroborate, and its free radical polymerization in the presence of azobisisobutyronitrile (AIBN) in dimethylformamide (DMF) at 100 °C gave rise to the porous polymer, POP-pNH_2Py, in quantitative yield. Methylation of POP-pNH_2Py with CH_3I in CH_3CN at 80 °C, followed by ion exchange with NaCl solution successfully yielded PQA-pNH_2Py-Cl (Fig. 1). X-ray photoelectron spectroscopy (XPS) data were recorded on

ESCALAB 250Xi with the Al Kα radiation, and energy calibration based on surface contamination C1s (284.8 eV) was applied to analyze the materials with XPS peak.

Commercial GAC (Filtrasorb® 400) was obtained from Calgon Carbon Co. The characteristics of the POP and GAC are presented in Table S2.

2.3. Adsorption experiments

The adsorption experiments were performed at the bench scale using a GYROMAX 818 shaker operating at 120 rpm. Samples were collected and filtered through a 0.2 μm membrane filter. All the following experiments were performed in duplicate at an ambient laboratory temperature of 23 °C. The results are presented as mean with the corresponding standard deviations.

2.3.1. Adsorption kinetics

Batch kinetics were performed at the initial PFAS solution (DI water spike with PFAS) concentration of 400 ng/L with an adsorbent dosage of 100 mg/L. To evaluate the adsorption rate, GAC was added into PFAS solution, shaking 2 h, 6 h, 12 h, 24 h, 36 h, 48 h, and 72 h; the POP was added into PFAS solution, shaking 5 min, 10 min, 15 min, 20 min, 30 min, 40 min, and 1 h.

Adsorption kinetics is expressed as the rate of adsorbate removal from the liquid phase to the adsorbent at a given condition. Equations (1) and (2) correspond to the pseudo-first-order and pseudo-second-order models, respectively, which were utilized to estimate the rate of adsorption (Ho and McKay, 1999).

$$q_t = q_e \bullet \left(1 - e^{-k_1 t}\right) \tag{1}$$

$$q_t = \frac{q_e^2 \bullet k_2 \bullet t}{1 + q_e \bullet k_2 \bullet t} \tag{2}$$

where q_e is the amount of PFAS adsorbed per unit mass of adsorbent at equilibrium, ng PFAS/g adsorbent; q_t is the amount of PFAS adsorbed per unit mass of adsorbent at time t, ng/g; k_1 is the pseudo-first-order rate constant, 1/h; k_2 is the pseudo-second-order rate constant, g/(ng•h); t is the time, h. The parameters of q_e and k_1 or q_e and k_2 were determined by fitting to the experimental data using non-linear regression. The amount of PFAS adsorbed per unit mass of adsorbent at time t, q_t (ng/g), is calculated by Equation (3):

$$q_t = \frac{(c_i - c_t) \bullet V}{m} \tag{3}$$

where c_i is the initial liquid phase PFAS concentration, ng PFAS/L; c_t is the liquid phase PFAS concentration at time t, ng/L; V is the volume of PFAS solution, L; m is the amount of adsorbent, g.

2.3.2. Adsorption isotherms

Batch isotherm experiments were carried out by adding various doses of adsorbents. 125 mL PET bottles were filled with 100 mL PFAS solution at the concentration of 400 ng/L and 0.005 g, 0.01 g, 0.02 g, 0.03 g, and 0.04 g adsorbent were added separately. To achieve equilibrium, the samples were mixed for 48 h for GAC and 15 min for POP, respectively, as determined by the results of the kinetic experiment.

Freundlich and Langmuir models were used frequently to describe the adsorption isotherms, as expressed in Equations (4) and (5) (Langmuir, 1916; Freundlich, 1926).

$$q_e = k_f \bullet c_e^{\frac{1}{n}} \tag{4}$$

$$q_e = \frac{q_m \bullet k_l \bullet c_e}{1 + k_l \bullet c_e} \tag{5}$$

where k_f is a Freundlich constant, $(ng/g)(L/ng)^{1/n}$; $1/n$ is the adsorption intensity; q_e is the amount of PFAS adsorbed per unit mass of adsorbent at equilibrium, ng PFAS/g; c_e is the liquid phase PFAS concentration at equilibrium, ng PFAS/L; k_l is a Langmuir constant associated with the strength of the adsorption binding energy, L/ng; q_m is the maximum adsorption capacity of the adsorbent, ng/g. The adsorption isotherm parameters, k_f and n, and q_m and k_l were determined by fitting to the experimental data using non-linear regression.

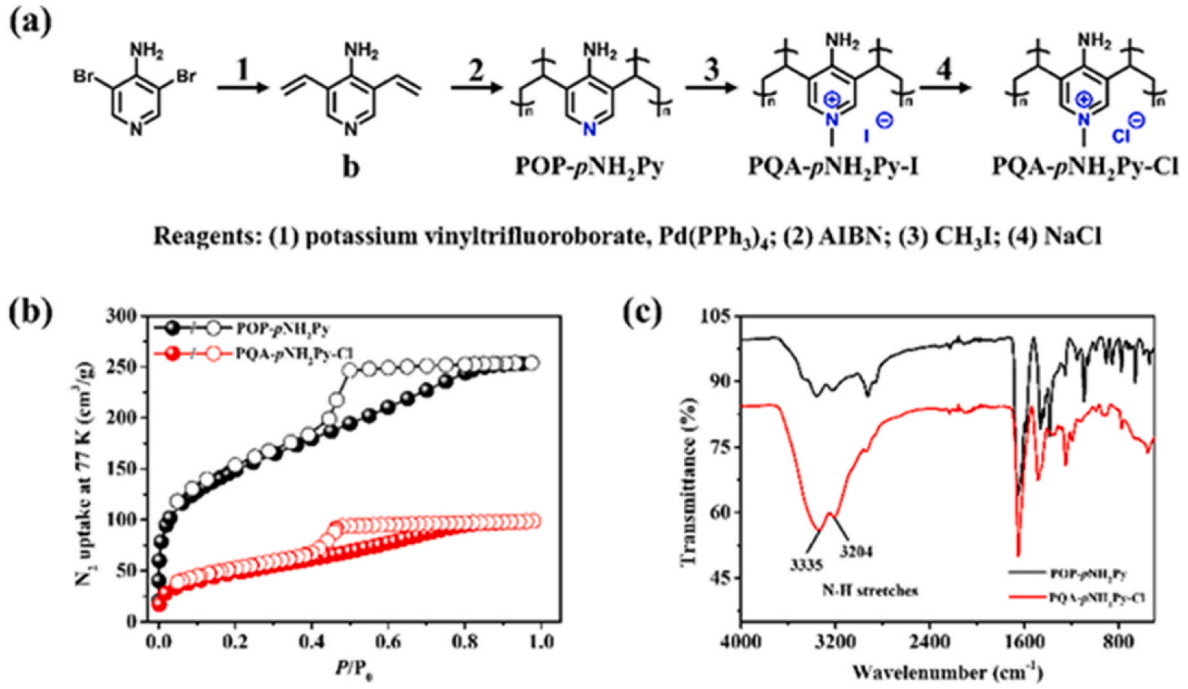

Fig. 1. (a) Synthesis of PQA-pNH$_2$Py-Cl, (b) N_2 adsorption/desorption isotherms of POP-pNH$_2$Py and PQA-pNH$_2$Py-Cl at 77 K, (c) FT-IR spectra of PO-pNH$_2$Py and PQA-pNH$_2$Py-Cl.

2.3.3. Effect of pH

Experiments were run under the normal range of pH in water systems (5–9) by adjustment with 0.1 M HNO_3 or NaOH to assess the influence of pH on the effectiveness of the POP for PFAS removal. A small volume (<0.5 mL) of HNO_3 or NaOH solution was added for pH adjustment. It had a negligible effect on the ionic strength (Yu et al., 2009; Zhang et al., 2021). Experiments were performed in 125 mL PET bottles containing 0.1 g/L of the POP and PFAS initial concentration of 400 ng/L. PFBA was selected as a representative short-chain PFAS for this testing.

The point of zero charges (pH_{PZC}) for an adsorbent surface refers to the pH at which the surface has a net neutral charge (Sposito, 1998). When the pH value is below the pH_{PZC}, there is an increased presence of protons, leading to the development of a positively charged surface on the adsorbent. Conversely, a negatively charged surface will be formed if the pH is above the pH_{PZC}. The batch mode study was conducted to determine the pH_{PZC} value for the POP. 15 mg of the POP was added in 20 mL of NaCl solution (0.1 M) and the initial pH value was adjusted to 2–12 by adding HCl (0.1 M) and NaOH (0.1 M). Samples were mixed on the shaker at 120 rpm and filtered by 0.45 μm filters. The final value of pH of the respective solution was measured and plotted against the initial pH. The pH_{PZC} was found to be the value at which the pH_{final} equals the $pH_{initial}$.

2.3.4. Effect of co-contaminants

Adsorption experiments were conducted in the presence of co-contaminants to determine how they affect the adsorption of short-chain PFAS onto the POP. Humic acid (HA) and fulvic acid (FA) are the predominant forms of organic matter (OM) in surface water, with concentrations ranging from 0.1 to 20 mg/L (Basumallick and Santra, 2017), chloride in the concentration range of 15–35 mg/L (Pal and Chakraborty, 2017), and long-chain PFAS in surface water and groundwater is typically in low ng/L to low μg/L range (Cordner et al., 2019; Kurwadkar et al., 2022). In this study, humic acid (HA), sodium chloride (NaCl), and PFOS were selected to represent the presence of OM, Cl^-, and the long-chain PFAS, respectively. Experiments were performed under varying POP dosages (0.05–0.4 g/L) with 8 mg/L HA (equivalent to 3.82 mg C/L), 30 mg/L Cl^-, 500 ng/L PFOS, and 400 ng/L PFBA.

The isotherm for multicomponent competitive adsorption can be modeled using Equation (6) based on single solute Freundlich isotherms (Sheindorf et al., 1981) or Equation (7) based on single solute Langmuir isotherms (Murali and Aylmore, 1983; Srivastava et al., 2006; Hilbrandt et al., 2019).

$$q_{e,i} = k_{f,i} \bullet c_{e,i} \left(\sum\nolimits_{j=1}^{n} \alpha_{i,j} c_{e,j} \right)^{(1/n_i)-1} \tag{6}$$

$$q_{e,i} = \frac{q_{m,i} k_{l,i} \left(c_{e,i}/\eta_i \right)}{1 + \sum_j^n k_{l,j} \left(c_{e,j}/\eta_j \right)} \tag{7}$$

where $k_{f,i}$ is the Freundlich constant for component i determined from single solute isotherm experiment, $(ng/g)(L/ng)^{1/n}$; $1/n_i$ is the adsorption intensity for component i determined from single solute isotherm experiment; n is the total number of components in the solution; $q_{e,i}$ is equilibrium adsorption capacity for component i, ng/g; $c_{e,i}$ and $c_{e,j}$ are the equilibrium concentrations for component i and j, ng/L; $k_{l,i}$ and $k_{l,j}$ are the Langmuir constants for component i and j determined from single solute isotherm experiment, L/ng; $q_{m,i}$ is the saturated maximum monolayer adsorption capacity for component i determined from single solute isotherm experiment, ng/g; $\alpha_{i,j}$ is the constant to describe the inhibition of component j on the adsorption of component i, unitless; η_i and η_j are interaction factors for component i and j, respectively. The parameters α and η were obtained by fitting to the experimental values of q_e and c_e by non-linear regression analysis.

2.4. Regeneration experiments

10 mg POP was added to a PET bottle in contact with 100 mL solutions of PFAS with an initial concentration of 400 ng/L. After adsorption experiments, the spent POP was separated by centrifugation. During the regeneration studies, the spent POP was put in a PET bottle with 100 mL of different regeneration solution to find the appropriate regeneration conditions. A solution containing 5% or 10% sodium chloride (NaCl) with 0%, 10%, 30%, 50%, and 70% methanol was used to regenerate the spent POP. The regeneration experiments were carried out at room temperature and 120 rpm in an shaker for 24 h. The concentration of PFAS in the supernatant of the regeneration solution was then analyzed. To test the reusability of the POP, the adsorption-regeneration experiments were conducted for five cycles and for each cycle the spend POP was regenerated by appropriate regeneration solution. The regeneration efficiency was determined by the ratio of the mass desorbed during the single cycle to the accumulated mass. The regeneration efficiency can be calculated by Equation (8):

$$\text{Regeneration efficiency } (\%) = \frac{q_{desorbed,n}}{\sum_{i=1}^{n} q_{adsorbed,i} - \sum_{j=1}^{n-1} q_{desorbed,j}} * 100\% \tag{8}$$

2.5. Analytical methods

PFAS samples were measured following EPA method 8327, which required the dilution of non-potable water samples with an organic solvent before conducting PFAS analysis. The experimental setup for this study used an Agilent 1260 HPLC coupled with an Agilent LC/MS QqQ 6460 system. Agilent ZORBAX RRHD Stable Bond C18, 100 × 2.1 mm, 1.8 μm and Agilent ZORBAX RRHD Eclipse Plus C18, 50 × 3.0 mm, 1.8 μm were used as analytical column and isolation column, respectively. A detailed description of the LC and MS conditions is provided in Table S3. Prior to analysis, the calibration curve was developed with the standards ranging from 5 to 500 ng/L. Isotopically labeled internal standards were added to all samples. A 30 μL aliquot of sample was injected into the analytical column. PFAS measurements were conducted using electrospray ionization in negative mode (ESI-) in multiple reaction monitoring (MRM) modes.

To determine the optimal wavelength for measuring the concentration of HA in a sample, absorbance was measured at various wavelengths (190–1100 nm) using an Agilent Cary 60 UV–Vis spectrophotometer. It showed that the absorbance at UV wavelengths between 340 and 600 nm (340, 360, 380, 400, 450, 500, 550, 600 nm) provided a reliable indication of HA. Notably, the wavelength at 400 nm exhibited the highest absorbance values, which corresponded to the maximum absorption peak of HA. Therefore, the calibration curve was developed with the standards ranging from 2 to 10 mg HA/L at this wavelength for measuring HA concentration. The major anion (Cl^-) in water was determined using ion chromatography. The pH was measured by Thermo Scientific pH meters.

3. Results and discussion

3.1. Design, synthesis, and characterization of POP

The Brunauer-Emmett-Teller (BET) surface area of PQA-*p*NH_2Py-Cl, calculated from the N_2 adsorption isotherm recorded at 77 K, is 172 $m^2\ g^{-1}$, much smaller than that of POP-*p*NH_2Py (521 $m^2\ g^{-1}$), indicative of the successful functionalization of the latter (Fig. 1b). Two types of pores were found in PQA-*p*NH_2Py-Cl (Fig. S2), with the sizes of 13 and 28 Å, respectively, indicating its hierarchical pore structure. The FT-IR spectrum of PQA-*p*NH_2Py-Cl clearly shows stretch vibrations at approximately 3335 and 3204 cm^{-1}, which are indicative of the presence of $–NH_2$ groups within the material's pores (Fig. 1c). Besides, the ζ potential of the aqueous suspensions of PQA-*p*NH_2Py-Cl is strongly

positive, indicative the cationic nature of the framework of the PQA-*p*NH_2Py-Cl (Table S2). These data confirmed the porous and cross-linked nature of the POP, which was then used to remove short-chain and branched PFAS from water.

3.2. PFAS removal kinetics by POP and GAC

The results from batch adsorption kinetic tests of PFAS by GAC and POP are described in Fig. 2 (a) and (b) . It was found that the adsorption of PFAS by GAC was slow, and adsorption equilibrium was achieved at 48 h. Compared with GAC, the adsorption of PFAS by the POP was up to 86% in 5 min, and the adsorption achieved equilibrium in 15 min with a removal of 95% (Fig. S3). The rapid decrease in PFAS concentration during the initial phase can be attributed to the high availability of active sites on the surface of the POP. As the active sites become nearly saturated, the rate of PFAS adsorption is primarily governed by the pore diffusion of PFAS onto the inner surface of the POP. This leads to a slower removal of PFAS until equilibrium is reached (Zhang et al., 2020).

The pseudo-first-order and pseudo-second-order models were used to describe the kinetic results to explore insight into the adsorption kinetics. Based on the results presented in Fig. 2 (a) and (b) and Table S4, the adsorption of PFAS onto the adsorbents was well-fit by the pseudo-second-order kinetic model. The correlation coefficient (R^2) values are all greater than 0.94. The adsorption rate constant of long-chain PFAS (PFOS) onto the POP is much lower compared to short-chain PFAS (PFBS, PFBA, PFHxA, and PFHpA). The faster adsorption rate for short-chain PFAS can be attributed to the smaller molecule having faster diffusion in pores, which is consistent with previous studies (Deng et al., 2010; Li et al., 2020). The corresponding pseudo-second-order rate constant k_2 for various PFAS adsorbed on the POP was in the range of 0.015–0.14 g/ng•h that was two orders of magnitude higher than that for PFAS adsorption on GAC (k_2 in the range of 0.00018–0.00091 g/ng•h as shown in Table S4). The time to reach adsorption equilibrium is much shorter for the POP (15 min in this study) compared to GAC (48 h in this study), ion exchange resins (2–168 h) (Dixit et al., 2021; Maimaiti et al., 2018; Vu and Wu, 2020), and other reported adsorbents (0.5–172 h) (Clark et al., 2019; He et al., 2022). The outstanding performance of the POP was attributed to its proper pore diameter and cationic nanotraps. GAC has a high total pore volume, however, micropore accounts for 80% of the total pore volume (Table S2), leading to a slow diffusion rate due to the pore blockage effect. Therefore, selecting the appropriate pore size distribution of an adsorbent is important to optimize the adsorption rate for the target PFAS contaminants.

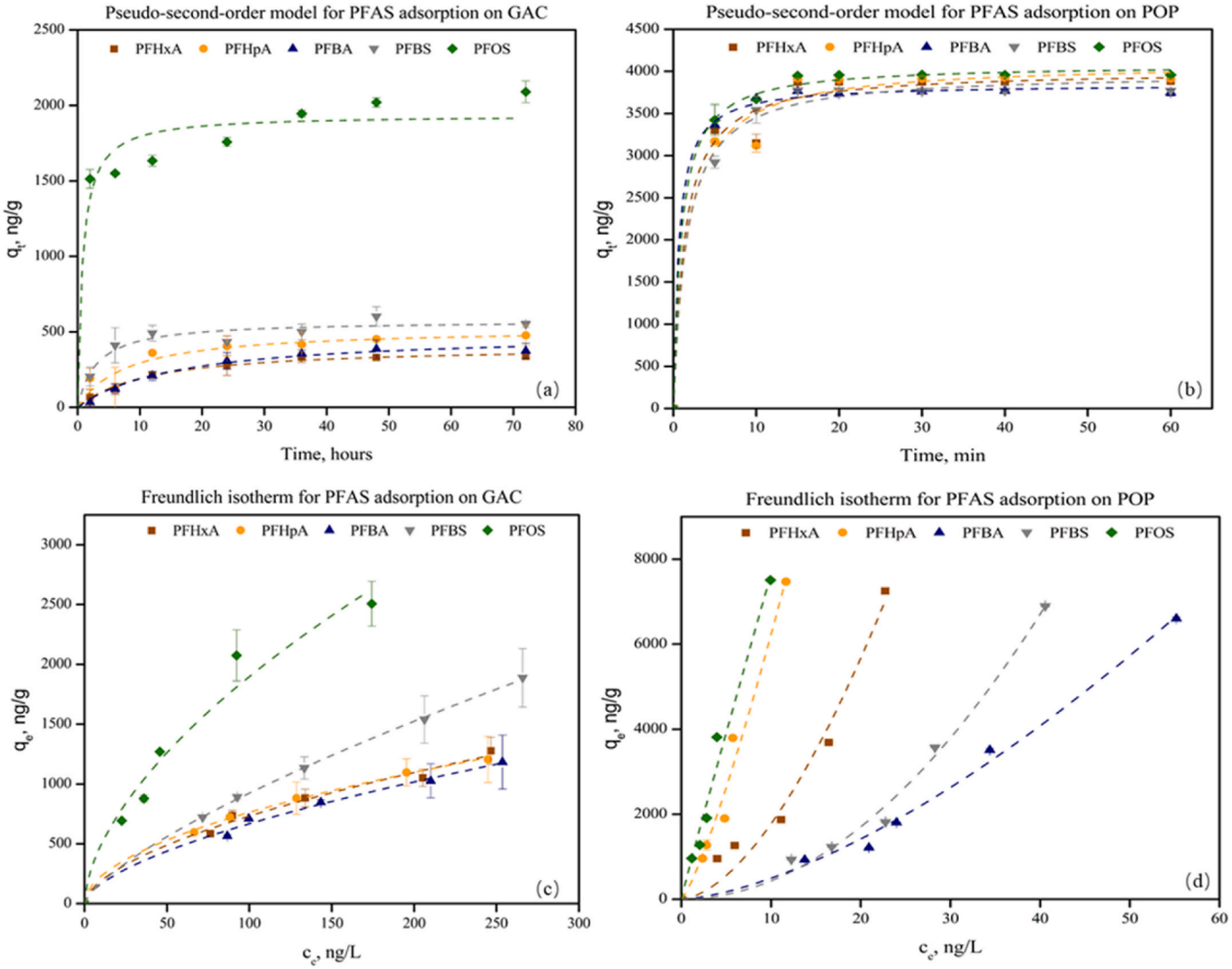

Fig. 2. Adsorption isotherms and kinetics. Pseudo-second-order model for the adsorption kinetics of PFAS onto (a) GAC and (b) POP. Freundlich model for the adsorption isotherms of PFAS onto (c) GAC and (d) POP.

3.3. PFAS removal isotherms by POP and GAC

Equilibrium isotherms are important for determining the maximum adsorption capacity of adsorbents and understanding interactions between PFAS and the POP. As shown in Fig. 2 (c) and (d), the removal of PFAS increased as the POP dose increased, primarily due to the increased adsorptive surface area and the availability of active adsorption sites. Comparing Langmuir and Freundlich isotherm models, Freundlich models better describe the adsorption isotherms of both long-chain and short-chain PFAS, indicating possible multilayer adsorption onto the POP and GAC. For GAC, the maximum adsorption capacity to remove short-chain PFAS (33.81, 37.70, 48.98, and 49.51 $(ng/g)(L/g)^{1/n}$ for PFBS, PFBA, PFHxA, and PFHpA) is limited compared to long-chain PFAS (90.47 $(ng/g)(L/g)^{1/n}$ for PFOS) as expected (Table S5). The maximum adsorption capacity of the POP for PFOS, PFBS, PFBA, PFHxA, and PFHpA was 737.39, 104.27, 157.77, 175.71, and 318.86 $(ng/g)(L/g)^{1/n}$, respectively (Table S5). Compared with GAC, the POP exhibited the adsorption capacity 8 times higher for long-chain PFAS and 3–6 times higher for short-chain PFAS. It is noteworthy that 1/n values for GAC are lower than 1, indicating the adsorption process is favorable and exhibits positive cooperativity. However, in this study, 1/n values for POP were higher than 1. This is because the isotherm experiments conducted in this study were at low concentrations (around 400 ng/L) and PFAS compounds tested contain polar functional groups, leading to potential competition with water for adsorption sites (Alimohammadi et al., 2017). A less favorable adsorption process leads to limited adsorption capacity, indicating that adsorption efficiency may be underestimated, particularly at low concentrations. Nonetheless, it is worth noting that the POP still exhibits high adsorption capacities. The results demonstrate that the POP is one of the promising PFAS adsorbent for short-chain and long-chain PFAS, especially at environmentally relevant concentrations and conditions. The cationic nanotraps in the framework can capture the anionic carboxylic or sulfonic groups, and the amino groups can form hydrogen bonding interactions with $–CF_2$-. Additionally, the aliphatic part in the framework can form hydrophobic interactions with the hydrophobic tail of PFAS.

Fig. 3 (a) presents the FT-IR spectra of PFBA, POP-Py-*p*-NH_2-CH_3Cl, and POP-Py-*p*-NH_2-CH_3Cl@PFBA. The FT-IR spectrum of POP-Py-*p*-NH_2-CH_3Cl@PFBA shows characteristic peaks of PFBA that are not present in the spectrum of POP-Py-*p*-NH_2-CH_3Cl, suggesting that PFBA is adsorbed into the pores of POP-Py-*p*-NH_2-CH_3Cl. When comparing the free PFBA with the PFBA inside the pores of the POP, the peaks that belong to the stretching vibration of the -O-H group (3510 cm^{-1}) disappear. This indicates that the –COOH of PFBA loses a proton in the aqueous solution and exists in the form of –COO–. This form can undergo ion exchange with Cl^- ions in the POP channel. After being absorbed into the POP channels, the vibrations of the C–C single bonds show a red shift of 4 cm^{-1}, while the vibrations of the asymmetric stretching of -C-F bonds show a red shift of 6 and 4 cm^{-1}, respectively. By comparing the infrared spectra of POP-Py-*p*-NH_2-CH_3Cl@PFBA and POP-Py-*p*-NH_2-CH_3Cl, the vibration of $–NH_2$ undergoes a red shift of 4 cm^{-1}. Therefore, the hydrogen bonding interaction between $–NH_2$ and -C-F bonds in PFBA is the main reason for the red-shift in the infrared spectral characteristic peaks of these bonds. This interaction leads to the decrease of the force constant of the $–NH_2$ and -C-F bond, which causes the red shift in the infrared spectrum (Mary et al., 2021).

The XPS analysis was conducted to determine the adsorption site of PFBA on POP-Py-*p*-NH_2-CH_3Cl, as shown in Fig. 3 (b) and (c). The analysis revealed that after the adsorption of PFBA, the Cl 2p peak in POP-Py-*p*-NH_2-CH_3Cl@PFBA disappeared, while the F 1s peak increased significantly. This indicates that an ion exchange process occurred between Cl^- and PFBA during the adsorption process.

3.4. Effect of pH on PFAS removal

Solution pH may affect the adsorption of PFAS by changing both the adsorbent surface charge and adsorbate species. The PFAS removal by the POP was evaluated under the normal range of pH (5–9) in water systems. As shown in Fig. 4 (a), the removal efficiency for PFOS and PFBA decreased with the increase in initial solution pH. The removal efficiency was up to 98% and 94% at pH 5 for PFOS and PFBA respectively, and decreased to 89% and 85% when the pH of the solution increased to 9. The same reduction in the removal efficiency was associated with the mechanism of electrostatic interactions influenced by pH change.

The acid dissociation constant (pKa) for adsorbate and the pH_{PZC} for adsorbent are the main parameters in describing the effect of pH on PFAS adsorption (Priyadarshini et al., 2022). Typically, most PFAS exist in the anionic form across a wide range of pH values due to their low pKa values (from −3.27 to 0.4) (Brooke et al., 2004; Goss, 2008). The

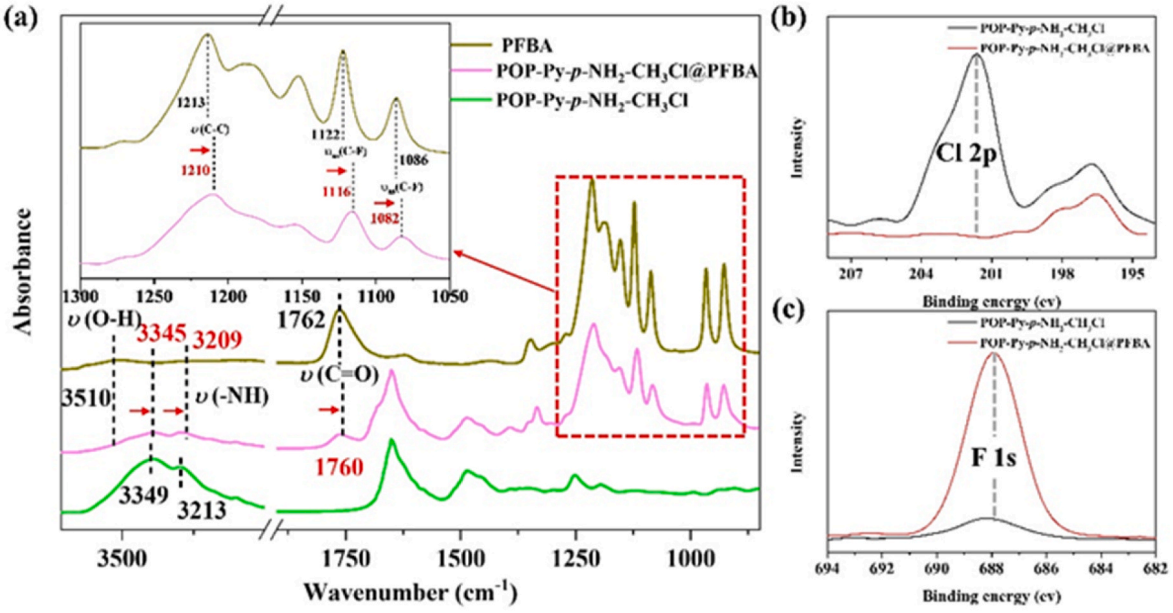

Fig. 3. (a) FT-IR spectra of PFBA, POP-Py-*p*-NH_2-CH_3Cl, and POP-Py-*p*-NH_2-CH_3Cl@PFBA, (b) Cl 2p XPS spectra for POP-Py-*p*-NH_2-CH_3Cl, and POP-Py-*p*-NH_2-CH_3Cl@PFBA, (c) F 1s XPS spectra for POP-Py-*p*-NH_2-CH_3Cl, and POP-Py-*p*-NH_2-CH_3Cl@PFBA.

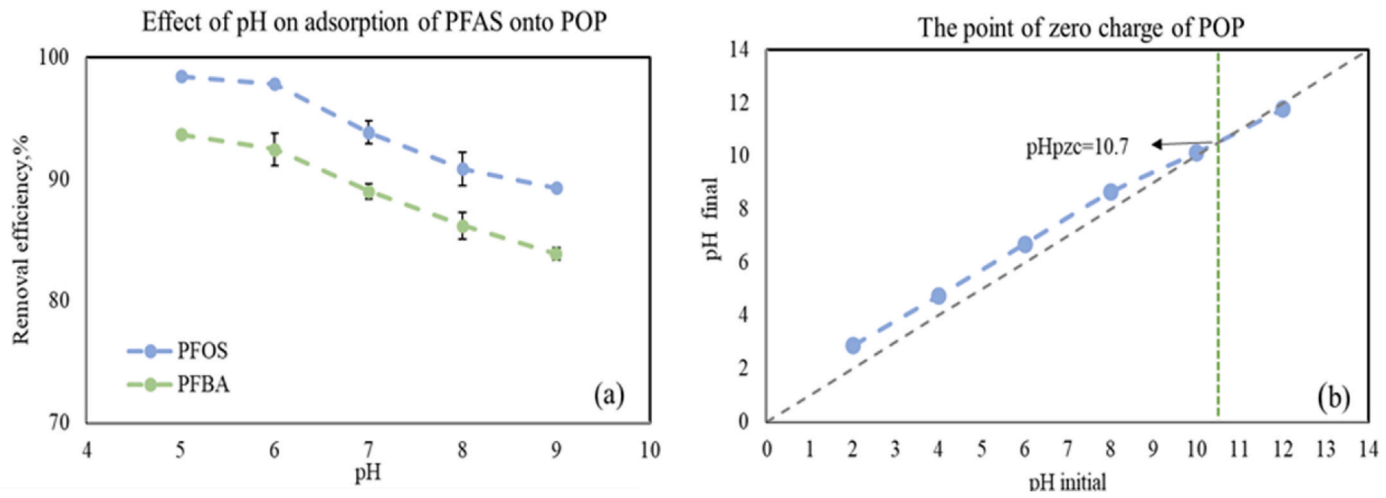

Fig. 4. (a)The effect of pH on the adsorption of PFBA and PFOS, and (b) the point of zero charge of the POP.

decrease in removal efficiency was attributed to the decrease in the number of positive active sites on the POP as the pH values increased. Experimentally, the pH_{PZC} value of the POP was found to be 10.7, as displayed in Fig. 4 (b). Accordingly, the surface of the POP behaves as positively charged at pH 5 to 9. Data from several previous studies suggested a negative correlation between the solution pH and the PFAS removal efficiency for POP (Liu et al., 2022a) and other adsorbents (Yang et al., 2020; Zhang et al., 2021; Boyer et al., 2021). However, the POP synthesized in this study maintained the high PFAS removal efficiency (above 85%) at pH 5 to 9. These findings indicate that there is no requirement for pH adjustment when using the POP, which can be advantageous for practical applications in the real world.

3.5. Effect of co-contaminants on PFAS removal

Competitive adsorption experiments were performed to determine the magnitude of competitive interaction among co-contaminants (PFOS, Cl^-, and HA) and PFBA. The competitive coefficients obtained by applying the Freundlich-type and Langmuir-type multicomponent isotherms are listed in Table 1. Note that for all the involved co-contaminants, the single solute isotherms conformed to a Freundlich model ($R^2 > 0.93$) (Table 1). The Freundlich-type multicomponent model had a good fit with high R^2 values (>0.91) obtained for the binary solute systems (Table 1). The high correlation for the Freundlich-type multicomponent isotherm could be attributed to the fact that the single solute isotherm for all components in the matrices followed the Freundlich isotherm.

This study measured PFBA adsorption in the presence of HA, a common type of natural organic matter. It can be seen from Table 1 that the magnitude of HA competition on PFBA adsorption was more significant, with a competitive coefficient ($\alpha_{PFBA,\ HA}$) of 16.68, than PFBA competition on HA adsorption, with a competitive coefficient ($\alpha_{HA,\ PFBA}$) of 0.061. As shown in Fig. 5 and Fig. S4 (a), HA removal by the POP ranged from 17.0% to 84.9% at various dosages of the POP in the binary solute system (PFBA + HA), similar to the HA removal in the single solute system (HA only). However, compared with the HA-free system, the PFBA removal decreased by around 20% in the binary solute system (PFBA + HA) and ranged from 63.5% to 74%. The adsorption of PFBA would be limited because HA competed for the available active adsorptive sites on the POP in the binary solute system (PFBA + HA). In addition, HA can change the surface charge of the POP because it contains numerous carboxylic (–COOH) and phenolic functional groups (-OH), making POP less effective for PFBA adsorption. The accumulation of adsorbed HA on the POP surface may cause electrostatic repulsion of PFBA due to cumulative negative charge.

Table 1
Single and binary solute adsorption isotherm parameters.

Single solute system	Freundlich single solute isotherm			Langmuir single solute isotherm		
	k_f, (ng/g)(L/ng)$^{1/n}$	1/n	R^2	k_l, L/ng	q_m, ng/g.	R^2
HA	8.9×10^6	0.93	0.93	2.42	1.33×10^{11}	0.84
PFOS	737.39	1.03	0.96	9.91×10^{-3}	8.44×10^8	0.97
Cl^-	1.2×10^6	0.85	0.95	1.35	8.94×10^{10}	0.62
Binary solute system (j = component listed below)	**Freundlich-type multicomponent isotherm**			**Langmuir-type multicomponent isotherm**		
	$\alpha_{PFBA,j}$	$\alpha_{j,PFBA}$	R^2	$\eta_{PFBA,j}$	$\eta_{j,PFBA}$	R^2
HA	16.68	0.061	0.91	9.69	0.24	0.83
PFOS	5.73	0.17	0.96	4.19	0.36	0.75
Cl^-	0.38	2.68	0.95	3.26	0.41	0.69

HA showed the highest competitiveness, which was almost three times greater than the value for PFOS. The results showed that POP has a greater affinity for PFOS than PFBA because the value of $\alpha_{PFBA,\ PFOS}$ ($\alpha_{PFBA,\ PFOS} = 5.73$) was higher than that of $\alpha_{PFOS,\ PFBA}$ ($\alpha_{PFBA,\ PFOS} = 0.17$). In the presence of PFBA, the change in PFOS removal efficiency was negligible, and the POP maintained a high PFOS removal efficiency (>94%) in both single and binary solute systems, as shown in Fig. 5 and Fig. S4 (b). In contrast, PFOS significantly inhibited PFBA adsorption in the binary solute system (PFBA + PFOS), causing an approximate 14% reduction in the PFBA removal at various dosages of the POP. This is because long-chain PFAS have higher hydrophobicity compared to short-chain PFAS, leading to stronger hydrophobic interaction with the POP.

Compared with HA and PFOS, Cl^- exhibited lower competitiveness with PFBA adsorption, as indicated by its low $\alpha_{PFBA,\ Cl}$-value ($\alpha_{PFBA,\ Cl^-} = 0.38$). Additionally, the competitive coefficient values showed that PFBA was less affected than Cl^- in the binary solute system (PFBA + Cl^-) ($\alpha_{PFBA,\ Cl^-} < \alpha_{Cl^-,\ PFBA} = 2.68$), which is in agreement with the experiment observation made in this study. The Cl^- removal efficiency ranged from 23.4% to 43.6% with various dosages of the POP (Fig. S4(c)) in the single solute system (Cl^- only) and decreased to 1.4%–2.3% in the presence of PFBA (Fig. 5). The Cl^- removal efficiency decreased in the binary solute system because the PFBA would compete with Cl^- on the active site with a greater affinity for POP due to additional hydrophobic interaction. In this study, the presence of Cl^- did not significantly affect the adsorption of PFBA on the POP.

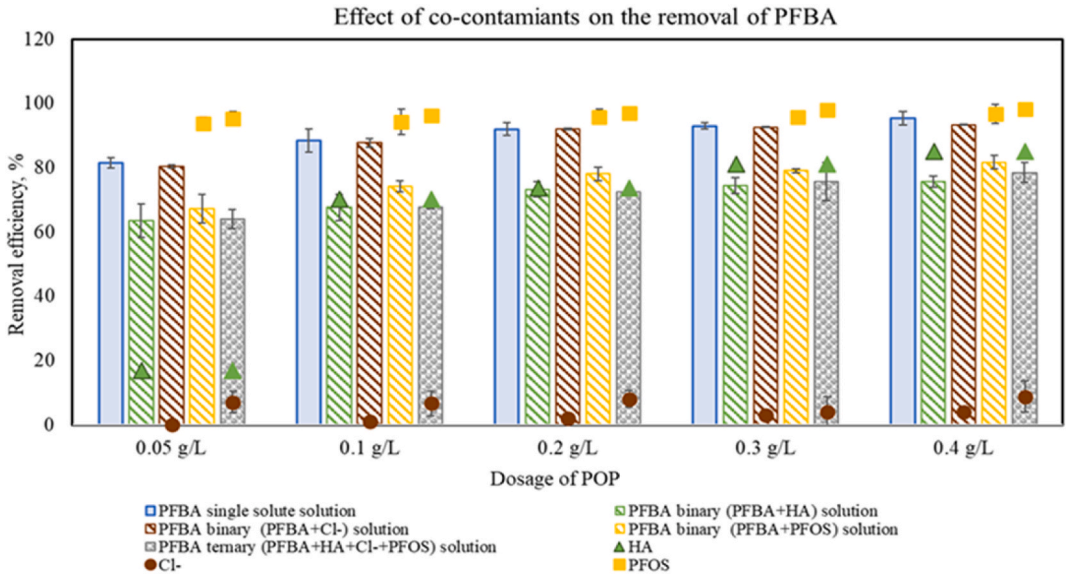

Fig. 5. Effect of co-contaminants on the removal of PFBA.

For the ternary solute system, the equilibrium adsorbent phase concentrations of PFBA at various dosages of the POP were estimated to be 618.53–3683.30 ng/g (Table S6 in the supplementary material) using the Freundlich-type multicomponent isotherm model with the competitive coefficient values in Table 1. These are consistent with the adsorbent phase PFBA concentration calculated from the experimental data with a relative error ranging from 1.1 to 11.3%, indicating a good model fit. In addition, the PFBA removal in the ternary solution system (63.5%–75.7%) was similar as the removal (61.9%–71.5%) in the binary solution of PFBA + HA (Fig. 5), indicating HA is the dominant co-contaminants for PFAB adsorption in the ternary solution. Overall, the multicomponent isotherm showed that co-contaminant inhibition effect on PFBA adsorption followed the order of HA > PFOS > Cl^-. To ensure effective treatment of PFAS-contaminated water, it is essential to remove OM and long-chain PFAS before short-chain PFAS removal.

3.6. Reusability of POP

Adsorbent regeneration is a significant characteristic in sustainable and cost-effective water treatment applications. To find an efficient while practical regeneration condition, methanol from 0 to 70% in the presence of 5% and 10% NaCl was explored. Fig. 6 shows regeneration efficiency of the POP for each PFAS with different regeneration solutions. Long-chain PFOS exhibits lower regeneration efficiency than short-chain PFAS. This distinction arises from the fact that long-chain PFAS molecules are more challenging to regenerate because their adsorption mechanism is hydrophobic interactions. In contrast, short-chain PFAS adsorption predominantly relies on electrostatic interactions and anion exchange processes, which likely explains their better regeneration performance compared to the long-chain PFOS.

The results showed that solutions of pure NaCl were unable to regenerate the POP. When NaCl concentration increased from 5% to 10% in DI water, they were still ineffective for desorbing PFAS from the POP because PFAS has low water solubility at high salt concentrations and ionic strengths (Chularueangaksorn et al., 2013). Using a mixture of NaCl and methanol, it was observed that the regeneration efficiency of the POP significantly improved from 1.1% to 90.1% as the concentration of methanol in the regeneration solution increased from 0 to 70% in the presence of 10% NaCl. The adsorbed PFAS was first desorbed from the binding sites on the adsorbent surface and then dissolved in solution as methanol enhances the solubility of PFAS.

The results showed that a higher concentration of the regenerant salts contributed to an improved regeneration efficiency. Specifically, the regeneration efficiency of the POP increased from 71.8% to 90.7% when NaCl increased from 5% to 10% in the presence of 30% methanol. However, increasing the methanol concentration to 70% only slightly

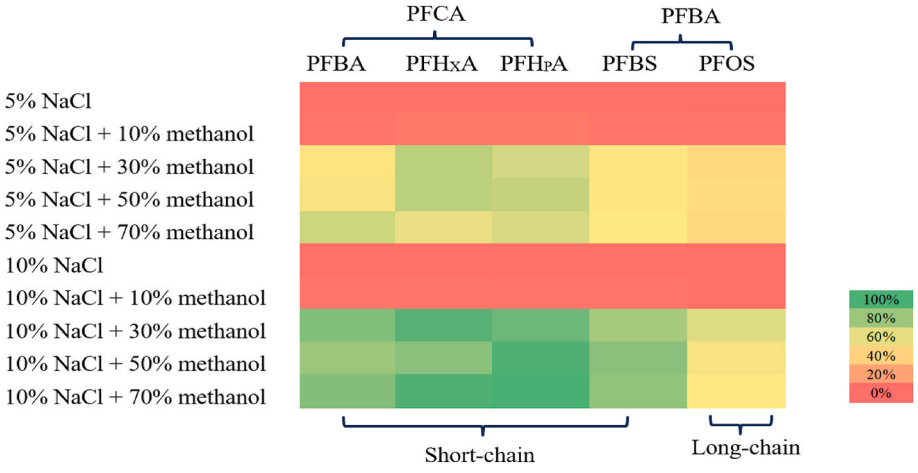

Fig. 6. The regeneration efficiency for each PFAS-loaded POP with different conditions.

improved POP regeneration. The obtained results are consistent with previous studies indicating that the addition of organic solvents to the NaCl regenerant has a limited impact on enhancing PFAS desorption when the organic solvent concentration exceeds 50% (Liu and Sun, 2021; Gao et al., 2017). Considering the challenges associated with using high percentages of organic solvents in large-scale water treatment, this study identified the combination of 10% NaCl and 30% methanol as the most efficient option for regenerating PFAS-loaded POP.

Fig. S6 illustrates the regeneration and adsorption efficiency of the POP using 10% NaCl in 30% methanol (the optimal condition found in this study). The performance of the POP did not decrease significantly and maintained high recovery and removal efficiency after five cycles. Compared with the first cycle, the removal efficiency of the POP decreased by 0.05%, and the regeneration efficiency decreased by 2.1% in the last cycle. These results demonstrate the promising potential of the POP as an adsorbent for PFAS removal due to its stable and high adsorption and regeneration capabilities.

4. Conclusion

In this study, a dual-functional POP, PQA-pNH_2Py-Cl, with cationic nanotraps, amino functional groups, and aliphatic part in the framework was investigated to remove PFAS under realistic environmental conditions. PQA-pNH_2Py-Cl has high adsorption capacities for both long-chain and short-chain PFAS, exhibiting fast kinetics and achieving equilibrium in less than 15 min. The impact of pH on the performance of the POP was minimal across the pH range typically found in natural waters. However, future studies should investigate a wider pH range, including values exceeding 10.7, to assess the performance of POPs across all potential pH conditions and prove the electrostatic interaction as one of the main mechanisms for PFAS adsorption using the POP. The inorganic anion (Cl^-) hardly interfered with PFBA removal, while organic matter (HA) and long-chain PFAS (PFOS) significantly decreased the adsorbed amount of PFBA. In addition, outstanding reusability of the POP was demonstrated with the optimal regeneration condition after five consecutive adsorption and desorption cycles. These impressive performance properties make PQA-pNH_2Py-Cl a promising and stable adsorbent for water treatment, enabling the fast and effective removal of PFAS, particularly short-chain PFAS under realistic environmental conditions.

Author contribution statement

Yan Zhang: Conceptualization, Methodology, Investigation, Writing – original draft, Visualization. **Bin Wang:** Conceptualization, Methodology, Resources, Writing – original draft, Visualization. **Shengqian Ma:** Supervision, Project administration. **Qiong Zhang:** Conceptualization, Methodology, Writing – review & editing, Supervision, Project administration.

Declaration of competing interest

The authors declare that they have no known competing financial interests or personal relationships that could have appeared to influence the work reported in this paper.

Data availability

Data will be made available on request.

Appendix A. Supplementary data

Supplementary data to this article can be found online at https://doi.org/10.1016/j.chemosphere.2023.140600.

References

Alimohammadi, M., Saeedi, Z., Akbarpour, B., Rasoulzadeh, H., Yetilmezsoy, K., Al-Ghouti, M.A., et al., 2017. Adsorptive removal of arsenic and mercury from aqueous solutions by eucalyptus leaves. Water, Air, Soil Pollut. 228, 1–27.

Ateia, M., Maroli, A., Tharayil, N., Karanfil, T., 2019. The overlooked short-and ultrashort-chain poly-and perfluorinated substances: a review. Chemosphere 220, 866–882.

Basumallick, S., Santra, S., 2017. Monitoring of ppm level humic acid in surface water using ZnO–chitosan nano-composite as fluorescence probe. Appl. Water Sci. 7, 1025–1031 [CrossRef Exact].

Boyer, T.H., Fang, Y., Ellis, A., Dietz, R., Choi, Y.J., Schaefer, C.E., et al., 2021. Anion Exchange Resin Removal of Per-And Polyfluoroalkyl Substances (PFAS) from Impacted Water: A Critical Review, vol. 200. Water research, 117244 [External Pubmed Partial][Check "stl" wrongly styled as "sbtl"].

Brendel, S., Fetter, É., Staude, C., Vierke, L., Biegel-Engler, A., 2018. Short-chain Perfluoroalkyl Acids: Environmental Concerns and a Regulatory Strategy under REACH. Environmental Sciences [External Pubmed Partial][Check punctuation in snm_2, , Check "atl" wrongly styled as "btl"].

Brooke, D., Footitt, A., Nwaogu, T.A., 2004. Environmental Risk Evaluation Report: Perfluorooctanesulphonate (PFOS), vol. 1. Environmental Agency [Not Available in CrossRef][Not Available in External Pubmed].

Chularueangaksorn, P., Tanaka, S., Fujii, S., Kunacheva, C., 2013. Regeneration and reusability of anion exchange resin used in perfluorooctane sulfonate removal by batch experiments. J. Appl. Polym. Sci. 130 (2), 884–890 [CrossRef Exact].

Chularueangaksorn, P., Tanaka, S., Fujii, S., Kunacheva, C., 2014. Batch and column adsorption of perfluorooctane sulfonate on anion exchange resins and granular activated carbon. J. Appl. Polym. Sci. 131 (3) [CrossRef Exact].

Clark, C.A., Heck, K.N., Powell, C.D., Wong, M.S., 2019. Highly defective UiO-66 materials for the adsorptive removal of perfluorooctanesulfonate. ACS Sustain. Chem. Eng. 7 (7), 6619–6628 [CrossRef Exact].

Cordner, A., De La Rosa, V.Y., Schaider, L.A., Rudel, R.A., Richter, L., Brown, P., 2019. Guideline levels for PFOA and PFOS in drinking water: the role of scientific uncertainty, risk assessment decisions, and social factors. J. Expo. Sci. Environ. Epidemiol. 29 (2), 157–171 [CrossRef Exact].

Crone, B.C., Speth, T.F., Wahman, D.G., Smith, S.J., Abulikemu, G., Kleiner, E.J., Pressman, J.G., 2019. Occurrence of per-and polyfluoroalkyl substances (PFAS) in source water and their treatment in drinking water. Crit. Rev. Environ. Sci. Technol. 49 (24), 2359–2396 [CrossRef Exact].

Deng, S., Yu, Q., Huang, J., Yu, G., 2010. Removal of perfluorooctane sulfonate from wastewater by anion exchange resins: effects of resin properties and solution chemistry. Water Res. 44 (18), 5188–5195 [CrossRef Exact].

Deng, S., Niu, L., Bei, Y., Wang, B., Huang, J., Yu, G., 2013. Adsorption of perfluorinated compounds on aminated rice husk prepared by atom transfer radical polymerization. Chemosphere 91 (2), 124–130 [CrossRef Exact].

Dickenson, E.R.V., Higgins, C., 2016. Treatment Mitigation Strategies for Poly-And Perfluoroalkyl Substances. WRF report, p. 4322 [Not Available in CrossRef][Not Available in External Pubmed].

Dixit, F., Dutta, R., Barbeau, B., Berube, P., Mohseni, M., 2021. PFAS removal by ion exchange resins: a review. Chemosphere 272, 129777 [CrossRef Exact].

Espana, V.A.A., Mallavarapu, M., Naidu, R., 2015. Treatment technologies for aqueous perfluorooctanesulfonate (PFOS) and perfluorooctanoate (PFOA): a critical review with an emphasis on field testing. Environ. Technol. Innovat. 4, 168–181 [CrossRef Exact].

Freundlich, H., 1926. Colloid & Capillary Chemistry. Methuen & co. ltd [Not Available in CrossRef][Not Available in External Pubmed].

Fujii, S., Polprasert, C., Tanaka, S., Hong Lien, N.P., Qiu, Y., 2007. New POPs in the water environment: distribution, bioaccumulation and treatment of perfluorinated compounds–a review paper. J. Water Supply Res. Technol. - Aqua 56 (5), 313–326 [CrossRef Exact].

Gagliano, E., Sgroi, M., Falciglia, P.P., Vagliasindi, F.G., Roccaro, P., 2020. Removal of poly-and perfluoroalkyl substances (PFAS) from water by adsorption: role of PFAS chain length, effect of organic matter and challenges in adsorbent regeneration. Water Res. 171, 115381 [CrossRef Exact].

Gao, Y., Deng, S., Du, Z., Liu, K., Yu, G., 2017. Adsorptive removal of emerging polyfluoroalky substances F-53B and PFOS by anion-exchange resin: a comparative study. J. Hazard Mater. 323, 550–557 [CrossRef Exact].

Goss, K.U., 2008. The p K a values of PFOA and other highly fluorinated carboxylic acids. Environ. Sci. Technol. 42 (2), 456–458 [CrossRef Exact].

He, J., Gomeniuc, A., Olshansky, Y., Hatton, J., Abrell, L., Field, J.A., Sierra-Alvarez, R., 2022. Enhanced removal of per-and polyfluoroalkyl substances by crosslinked polyaniline polymers. Chem. Eng. J. 446, 137246 [CrossRef Exact].

Hilbrandt, I., Lehmann, V., Zietzschmann, F., Ruhl, A.S., Jekel, M., 2019. Quantification and isotherm modelling of competitive phosphate and silicate adsorption onto micro-sized granular ferric hydroxide. RSC Adv. 9 (41), 23642–23651 [CrossRef Exact].

Ho, Y.S., McKay, G., 1999. Pseudo-second order model for sorption processes. Process Biochem. 34 (5), 451–465 [CrossRef Exact].

Houtz, E.F., Higgins, C.P., Field, J.A., Sedlak, D.L., 2013. Persistence of perfluoroalkyl acid precursors in AFFF-impacted groundwater and soil. Environ. Sci. Technol. 47 (15), 8187–8195 [CrossRef Exact].

Karoyo, A.H., Wilson, L.D., 2013. Tunable macromolecular-based materials for the adsorption of perfluorooctanoic and octanoic acid anions. J. Colloid Interface Sci. 402, 196–203 [CrossRef Exact].

Kucharzyk, K.H., Darlington, R., Benotti, M., Deeb, R., Hawley, E., 2017. Novel treatment technologies for PFAS compounds: a critical review. J. Environ. Manag. 204, 757–764 [CrossRef Exact].

Kurwadkar, S., Dane, J., Kanel, S.R., Nadagouda, M.N., Cawdrey, R.W., Ambade, B., et al., 2022. Per-and polyfluoroalkyl substances in water and wastewater: a critical review of their global occurrence and distribution. Sci. Total Environ. 809, 151003 [CrossRef Exact].

Langmuir, I., 1916. The constitution and fundamental properties of solids and liquids. Part I. Solids. J. Am. Chem. Soc. 38 (11), 2221–2295. https://doi.org/10.1021/ja02268a002 [CrossRef Exact].

Lau, C., Anitole, K., Hodes, C., Lai, D., Pfahles-Hutchens, A., Seed, J., 2007. Perfluoroalkyl acids: a review of monitoring and toxicological findings. Toxicol. Sci. 99 (2), 366–394 [CrossRef Exact].

Li, B., Zhang, Y., Ma, D., Shi, Z., Ma, S., 2014. Mercury nano-trap for effective and efficient removal of mercury (II) from aqueous solution. Nat. Commun. 5 (1), 5537 [CrossRef Exact].

Li, F., Duan, J., Tian, S., Ji, H., Zhu, Y., Wei, Z., Zhao, D., 2020. Short-chain per-and polyfluoroalkyl substances in aquatic systems: occurrence, impacts and treatment. Chem. Eng. J. 380, 122506 [CrossRef Exact].

Liu, Y.L., Sun, M., 2021. Ion exchange removal and resin regeneration to treat per-and polyfluoroalkyl ether acids and other emerging PFAS in drinking water. Water Res. 207, 117781 [CrossRef Exact].

Liu, G., Wei, X., Luo, P., Dai, S., Zhang, W., Zhang, Y., 2022a. Novel fluorinated nitrogen-rich porous organic polymer for efficient removal of perfluorooctanoic acid from water. Water 14 (7), 1010 [CrossRef Exact].

Liu, X., Zhu, C., Yin, J., Li, J., Zhang, Z., Li, J., et al., 2022b. Installation of synergistic binding sites onto porous organic polymers for efficient removal of perfluorooctanoic acid. Nat. Commun. 13 (1), 2132 [CrossRef Exact].

Maimaiti, A., Deng, S., Meng, P., Wang, W., Wang, B., Huang, J., et al., 2018. Competitive adsorption of perfluoroalkyl substances on anion exchange resins in simulated AFFF-impacted groundwater. Chem. Eng. J. 348, 494–502 [CrossRef Exact].

Mary, S.J.J., Siddique, M.U.M., Pradhan, S., Jayaprakash, V., James, C., 2021. Quantum chemical insight into molecular structure, NBO analysis of the hydrogen-bonded interactions, spectroscopic (FT–IR, FT–Raman), drug likeness and molecular docking of the novel anti COVID-19 molecule 2-[(4,6-diaminopyrimidin-2-yl)sulfanyl]-N-(4-fluorophenyl)acetamide - dimer. Spectrochim. Acta Mol. Biomol. Spectrosc. 244, 118825 [CrossRef Exact].

Meegoda, J.N., Kewalramani, J.A., Li, B., Marsh, R.W., 2020. A review of the applications, environmental release, and remediation technologies of per-and polyfluoroalkyl substances. Int. J. Environ. Res. Publ. Health 17 (21), 8117 [CrossRef Exact].

Meegoda, J.N., Bezerra de Souza, B., Casarini, M.M., Kewalramani, J.A., 2022. A review of PFAS destruction technologies. Int. J. Environ. Res. Publ. Health 19 (24), 16397 [CrossRef Exact].

Moldes, Moriwaki, H., Takagi, Y., Tanaka, M., Tsuruho, K., Okitsu, K., Maeda, Y., 2005. Sonochemical decomposition of perfluorooctane sulfonate and perfluorooctanoic acid. Environ. Sci. Technol. 39 (9), 3388–3392 [CrossRef Exact].

Murali, V., Aylmore, L.A.G., 1983. Competitive adsorption during solute transport in soils: 1. Mathematical models. Soil Sci. 135 (3), 143–150 [CrossRef Exact].

Pal, S., Chakraborty, K., 2017. Different aspects of chloride in freshwater: a review. Int. J. Curr. Trends in Sci. Technol. 7 (8), 20295–20303 [Not Available in CrossRef][Not Available in External Pubmed].

Priyadarshini, N., Das, K.K., Mansingh, S., Parida, K., 2022. Facile fabrication of functionalised Zr co-ordinated MOF: antibiotic adsorption and insightful physiochemical characterization. Results in Chem. 4, 100450 [CrossRef Exact].

Punyapalakul, P., Suksomboon, K., Prarat, P., Khaodhiar, S., 2013. Effects of surface functional groups and porous structures on adsorption and recovery of perfluorinated compounds by inorganic porous silicas. Separ. Sci. Technol. 48 (5), 775–788 [CrossRef Exact].

Rattanaoudom, R., Visvanathan, C., Boontanon, S.K., 2012. Removal of concentrated PFOS and PFOA in synthetic industrial wastewater by powder activated carbon and hydrotalcite. J. Water Sustain. 2 (4), 245–258 [Not Available in CrossRef][Not Available in External Pubmed].

Senevirathna, S.T.M.L.D., 2010. Development of Effective Removal Methods of PFCs (Perfluorinated Compounds) in Water by Adsorption and Coagulation [Not Available in CrossRef][Not Available in External Pubmed].

Sheindorf, C., Rebhun, M., Sheintuch, M., 1981. A Freundlich-type multicomponent isotherm. J. Colloid Interface Sci. 79 (1), 136–142 [CrossRef Exact].

Sposito, G., 1998. On points of zero charge. Environ. Sci. Technol. 32 (19), 2815–2819 [CrossRef Exact].

Srivastava, V.C., Mall, I.D., Mishra, I.M., 2006. Equilibrium modelling of single and binary adsorption of cadmium and nickel onto bagasse fly ash. Chem. Eng. J. 117 (1), 79–91 [CrossRef Exact].

Sun, Q., Zhu, L., Aguila, B., Thallapally, P.K., Xu, C., Chen, J., et al., 2019. Optimizing radionuclide sequestration in anion nanotraps with record pertechnetate sorption. Nat. Commun. 10 (1), 1646 [CrossRef Exact].

U.S. Environmental Protection Agency, 2023. National primary drinking water regulation for perfluorooctanoic acid (PFOA) and perfluorooctanesulfonic acid (PFOS) and a grouped MCL for perfluorohexanesulfonic acid (PFHxS), GenX chemicals, perfluorononanoic acid (PFNA), and perfluorobutanesulfonic acid (PFBS); proposed rule. Fed. Regist. 88 (51), 14466–14525. Retrieved from. https://www.epa.gov/system/files/documents/2023-03/PrePublication%20Federal%20Register%20Notice_PFAS%20NPDWR_NPRM_Final_3.13.23.pdf [Not Available in CrossRef][Not Available in External Pubmed].

Verma, S., Lee, T., Sahle-Demessie, E., Ateia, M., Nadagouda, M.N., 2022. Recent advances on PFAS degradation via thermal and nonthermal methods. Chem. Eng. J. Adv., 100421 [CrossRef Exact].

Vu, C.T., Wu, T., 2020. Adsorption of short-chain perfluoroalkyl acids (PFAAs) from water/wastewater. Environ. Sci.: Water Res. Technol. 6 (11), 2958–2972 [CrossRef Exact].

Wang, B., Lee, L.S., Wei, C., Fu, H., Zheng, S., Xu, Z., Zhu, D., 2016. Covalent triazine-based framework: a promising adsorbent for removal of perfluoroalkyl acids from aqueous solution. Environ. Pollut. 216, 884–892 [CrossRef Exact].

Wu, C., Klemes, M.J., Trang, B., Dichtel, W.R., Helbling, D.E., 2020. Exploring the factors that influence the adsorption of anionic PFAS on conventional and emerging adsorbents in aquatic matrices. Water Res. 182, 115950 [CrossRef Exact].

Yang, K., Xing, B., 2010. Adsorption of organic compounds by carbon nanomaterials in aqueous phase: polanyi theory and its application. Chem. Rev. 110 (10), 5989–6008 [CrossRef Exact].

Yang, A., Ching, C., Easler, M., Helbling, D.E., Dichtel, W.R., 2020. Cyclodextrin polymers with nitrogen-containing tripodal crosslinkers for efficient PFAS adsorption. ACS Mater. Lett. 2 (9), 1240–1245 [CrossRef Exact].

Yu, J., Hu, J., Tanaka, S., Fujii, S., 2009. Perfluorooctane sulfonate (PFOS) and perfluorooctanoic acid (PFOA) in sewage treatment plants. Water Res. 43 (9), 2399–2408 [CrossRef Exact].

Zhang, D.Q., Zhang, W.L., Liang, Y.N., 2019. Adsorption of perfluoroalkyl and polyfluoroalkyl substances (PFASs) from aqueous solution-A review. Sci. Total Environ. 694, 133606 [CrossRef Exact].

Zhang, T., Xing, G., Chen, W., Chen, L., 2020. Porous organic polymers: a promising platform for efficient photocatalysis. Mater. Chem. Front. 4 (2), 332–353 [CrossRef Exact].

Zhang, J., Pang, H., Gray, S., Ma, S., Xie, Z., Gao, L., 2021. PFAS removal from wastewater by in-situ formed ferric nanoparticles: solid phase loading and removal efficiency. J. Environ. Chem. Eng. 9 (4), 105452 [CrossRef Exact].

Zhang, Z., Sarkar, D., Datta, R., Deng, Y., 2021. Adsorption of perfluorooctanoic acid (PFOA) and perfluorooctanesulfonic acid (PFOS) by aluminum-based drinking water treatment residuals. J. Hazard. Mater. Lett. 2, 100034 [CrossRef Exact].